Proceedings of ASME 2020
3rd International Offshore Wind Technical Conference
IOWTC2020
October 18-21, 2020, Boston, MA, USA

IOWTC2020-3503

A REDUCED-ORDER MATHEMATICAL MODEL FOR THE CURRENT-INDUCED MOTION OF A FLOATING OFFSHORE WIND TURBINE

Éverton L. de Oliveira[1], Celso P. Pesce[2], Bruno Mendes[2], Renato M. M. Orsino[2] and Guilherme R. Franzini[2]

[1] Dynamics and Control Laboratory
[2] Offshore Mechanics Laboratory
Escola Politécnica, University of São Paulo, São Paulo, Brazil

ABSTRACT

Floating offshore platforms motions induced by currents are quite complex phenomena, in general. In particular, VIM, Vortex-Induced Motion, is a type often encountered in platforms with circular columns. Recently, VIM has been observed in towing tank tests with a small-scale model of a Floating Offshore Wind Turbine (FOWT), the OC4 Phase II floater, a 3+1 columns platform. The present paper proposes a reduced-order mathematical model (ROM) to assess VIM of a FOWT. The ROM is derived on the horizontal plane, including yaw motions and nonlinear mooring forces. Current forces are represented through 'wake variables', adapting phenomenological models firstly used for VIM of mono-column platforms. The ROM is built upon a set of eleven generalized coordinates, three for the rigid body motion on the horizontal plane and a pair of wake variables for each column, resulting in a system of eleven nonlinear second-order ODEs. The pairs of wake variables obey van der Pol equations, and use hydrodynamic coefficients and parameters obtained from previous experiments with small draught cylinders. Hydrodynamic interferences among columns or heave plates effects on the flow are not considered, for simplicity. The validity of the proposed model is assessed having the mentioned small-scale experimental campaign as a case study. The simulations are carried out at three different current incidence angles, 0, 90 and 180 degrees, spanning a large range of reduced velocities. The simulations reproduce well the oscillations observed in the experimental tests. A good agreement in transverse oscillations is found, including lock-in regions. The simulations also depict a possibly important phenomenon: a resonant yaw motion emerging at high reduced velocities.

Keywords: VIM, FOWT, Reduced-order Model, Wake Oscillator modeling, experimental comparison.

INTRODUCTION

Density of power, steadiness and enormous available oceanic areas have proved offshore wind as a promising renewable energy source. TLP, monocolumn and semisubmersible platforms, originally employed as solutions for the offshore oil and gas sector, have been used recently in the offshore wind energy industry to give support to wind turbines in mid and relatively deep waters, [1]. Such floating moored unities are acted by strong loads due to the incoming waves, wind and current. Ocean currents, generally quite steady flows, may be responsible not only for displacing the unit away from its original design position, but also for inducing slow oscillatory motions on the horizontal plane. In the case of floating platforms with circular columns, current induced motions are usually related to the vortex shedding phenomenon and are known as Vortex-Induced Motions (VIM). VIM is a recurrent phenomenon, what may turn its prediction an important issue in the design process; see, e.g., [2].

Generally speaking, VIM is a non-linear resonant phenomenon, of the Vortex-Induced Vibration (VIV) type, in which the frequency of the vortex structures, shed from vertical cylindrical bodies that constitute the hull, synchronize with the usually low natural frequencies of the system, corresponding to the oscillation modes of the moored platform on the horizontal plane.

Computational Fluid Dynamics modeling (CFD) might be used to solve the Navier-Stokes and the Poisson equations, which govern the velocity and pressure flow fields. Once coupled to the dynamic equations of the body, such a modeling technique might serve as a prediction tool for VIM. However, the high computational time of the numerical simulations usually impairs this approach, at least during design stages. Moreover, verification and validation procedures cannot be dispensed.

Alternatively, phenomenological models based on non-linear oscillators, such as on van der Pol equations, are proper to

vortex wake dynamics modeling. In fact, the non-linear self-sustained and self-excited mechanism of the vortex-shedding phenomenon resembles the response of such a class of oscillators, characterized by Hopf bifurcations and the existence of limit cycles. Indeed, Aranha (2004), [3], after the work by Huerre and Monkewitz (1990), [4], proved that the vortex wake dynamics behind slender fixed cylinders exposed to current flows, therefore affected by a weak three-dimensionality, is governed by Ginsburg-Landau oscillators which emerge naturally from the Navier-Stokes equations. Besides, as well-known, Landau equation is a particular case of the van der Pol equation, which can be also transformed into a Rayleigh oscillator. This class of phenomenological approach is also known as 'wake oscillators' modeling.

The interaction between the flow and the structure dynamics can be modelled through a proper coupling between the corresponding equations to emulate the classical VIV. Early studies on such a class of models, treating VIV of rigid cylinders mounted on elastic supports and free to move transversally to the income flow, may be traced back to the 1960's and 1970's; see, e.g., [5]. Iwan and Blevins' (1974) model, [6], is one of fundamental importance, in which coupling between the wake oscillator and the cylinder dynamics was made through velocity dependent terms. See, also, [7].

About thirty years later, comparing experimental and numerical results on classic VIV, Facchinetti and his collaborators, [8], concluded that the mentioned interaction might be modeled as dominated by inertial terms, proposing then a coupling in terms of acceleration. It is worth noticing that the dependence of coupling parameters on the variation of inertial terms, as the added mass taken as function of the reduced velocity, had been already considered, see, e.g., [9], by modifying the classic model of Iwan and Blevins. An acquaintance of the differences between models, regarding the robustness of the added mass concept on VIV, may be seen in [10]. Recently, the discussion on the added mass concept on VIV has regained a renewed strength, as shown by a novel reinterpretation of this complex phenomenon by Bernitsas et al, [11].

Facchinetti et al's model was revisited and discussed in detail by Ogink and Metrikine, [12]. Still restricted to one degree of freedom (1-dof) VIV, an important hypothesis of Facchinetti et al's model, namely, the linearization of the instantaneous relative velocity of the cylinder with respect to the flow, was relaxed. Moreover, the authors modified the coupling parameters, according to the experimentally observed vortex emission regime. More recently, Franzini and Bunzel, [13], extended the approach by Ogink and Metrikine to two degrees of freedom (2-dof), allowing both crosswise and in-line oscillations. A second van der Pol oscillator, vibrating twice as fast as the crosswise one, was introduced in the in-line direction, assuming, *a priori*, a dual ressonance phenomenon.

Aditionally, regarding calibration, CFD has been used, [14], to determine the parameters that govern some types of wake oscillator models. The influence of mass ratio was discussed, such as their impact on response amplitudes and on the width of the lock-in region.

Wake oscillator models have then been applied to monocolumn production, storage and offloading (MPSO) floating platforms, with success; see [15], [16]. In those papers, CFD techniques were applied to improve the adherence between the results of a wake-oscillator model with experiments. Using one van der Pol oscillator for vortex wake dynamics modelling and a linear oscillator with two degrees of freedom (2-dof) for the platform dynamics, a parametric analysis was carried out. Moreover, it was concluded that the three-dimensionallity of the flow due to the small aspect ratio of the floating monocolumn cylindrical platform has a strong influence on the frequency of vortex shedding, thus on the Strouhal number; see also [17].

Improving even more such kind of modelling to study VIM of a MPSO, [18] considered a two-wake oscillators model, based on Franzini and Bunzel's work. The very low aspect ratio of the cylindrical platform (~ 1:3) was duly taken into account by applying the proper and smaller Strouhal number, experimentally determined in [19]. A 5-dof reduced-order mathematical model (ROM) was then constructed. That model considered the platform dynamics in three degrees of freedom on the horizontal plane coupled to two van der Pol wake oscillators to deal with the VIM phenomenology. The use of two van der Pol oscillators, adapting the Franzini and Bunzel's model, [13], with proper parameters and coefficients, was the methodological difference of that work compared with [16]. Another key improvement was the consistent modelling of the nonlinear response of the mooring lines, using the closed-form analytical approach, based on methods of Analytical Mechanics, introduced by [20]. In fact, such an approach made it possible to observe yawing motions driven by the mooring lines while the body centroid develops classic eight shaped trajectories on the horizontal plane, even treating a circular cylindrical hull. A good comparison with experiments was then obtained.

Motivation and objectives

The good numerical results obtained in [18], and the recent experimental findings by Gonçalves et al, [21], on the existence of VIM on a small-scale multicolumn FOWT model, truly motivated the present work. The intent henceforth is to verify whether reduced-order models based on wake oscillators could be successfully applied to multicolumnar platforms.

The experiments reported in [21] were carried out with a small-scale model of the FOWT OC-4 (Phase 2) platform in a towing tank. That study proved VIM as a worthwhile investigation phenomenon for multicolumn FOWT platforms, at least in laboratory scale, where relatively low Reynolds numbers take place. If proved to be relevant in full scale, VIM might constitute a significant factor to the operation of wind turbines, especially in the case of substantial yaw oscillations, possibly affecting the azimuthal orientation control of the nacelle.

Regarding the mooring system, four pre-tensioned linear springs were perpendicularly arranged and connected to a circular rigid ring attached to the platform model. As already mentioned, geometric nonlinearities in the mooring restoring forces are relevant, inducing couplings between translational and yaw motions. Pesce et al's, [20], closed form formulation for the response of a generic mooring system shows explicitly the dependence of the restoring forces on the position and heading of the floating unit. Such analytical formulation, geometrically non-linear, is shown to be important for the conception of a consistent reduced-order model on the horizontal plane.

Gonçalves et al, [21], observed that the amplitudes of oscillation in the transverse direction to the incoming flow reached up to circa 60% of the diameter of the largest (and external) columns. This happened within the synchronization (lock-in) range varying between 5 and 10, with reduced velocities defined by taking the diameter of the external columns as the length scale. Such values, if extrapolated to the real scale, would refer to current speeds between 0.5 and 1.2 (m/s), often found in offshore areas.

The trajectories of the platform centroid experimentally observed on the horizontal plane depended on the incidence angle of the flow. Indeed, some differences were reported at 0 and 180 degrees. Notice that at these two incidence angles, columns are not aligned with the flow, which certainly reduces wake interferences between them. On the contrary, at 90 degrees incidence angle, the columns alignment with respect to the flow increases wake interferences.

In the present work, using the formalism of Analytical Mechanics and based on a wake oscillators phenomenological approach, a reduced-order mathematical model (ROM) is derived to assess the motion on the horizontal plane of multicolumnar floating platforms. The conceptual floater FOWT-OC-4 Phase II is used as a case study and numerical results are confronted with the experimental data presented in [21]. The authors believe that this is the first attempt to model VIM of a multicolumn floating platform through a ROM, by using the wake oscillator approach.

THE REDUCED-ORDER MATHEMATICAL MODEL

In this section, a reduced-order model is proposed for the problem under discussion. Lagrange's equations for the horizontal plane rigid-body motions (3-dof) of the platform are derived, neglecting coupling effects with out-of-plane motions. Hydrodynamic and mooring line restoring forces on the horizontal plane are taken as generalized forces.

The generalized mooring line restoring forces are modeled in a quite general way, through the formalism of Analytical Mechanics, following [20]. Such a derivation permits to consider rather distinct mooring configurations, taking nonlinearities into account. Restoring forces are considered to be function of position only, in a quasi-static approach. Effects associated with the mooring lines dynamics are not considered in this model, what should include 'mooring line damping', for instance. This issue certainly deserves a proper discussion, what is left for a future work, since not relevant to modeling the small-scale experiments in [21], as the mooring system was formed by springs in the air.

Two fluid-structure interaction effects are considered in this model: (i) the inertial ones, represented through the well-known concept of the potential added mass tensor; (ii) those related to the vortex shedding phenomenon, here represented via a phenomenological approach. For each column of the platform, the corresponding drag and lift forces coefficients are expressed as functions of two independent variables, each of them modelled according to a wake-oscillator, of the van der Pol type, forced by a term proportional to the respective component of acceleration in the direction of the current (in-line direction) and transversally to it (crosswise direction). These wake-oscillators represent two additional degrees of freedom for each column, which, along with the three degrees of freedom of rigid-body motions of the platform in the horizontal plane, totalize 11-dof. In the sequel, the governing equations for the dynamic of the platform are established.

Equations of motion on the horizontal plane

For simplicity, assume that the current has a uniform velocity profile both in magnitude U_∞ and direction. Define (O, X, Y) as a Cartesian coordinate system in the horizontal plane, attached to an inertial reference frame, whose X direction is parallel to the current. Let $\mathbf{q} = \begin{bmatrix} x & y & \psi \end{bmatrix}^T$ be the 3-vector of generalized coordinates that describe the rigid-body motions of the platform on the horizontal plane, with (x, y) representing the coordinates of the center A of the platform in (O, X, Y) and ψ denoting the *yaw* angle, as illustrated in Figure 1. Also, define (A, ξ, η) as a body-fixed coordinate system, that coincides with (O, X, Y) when $A \equiv 0$ and $\psi = 0$.

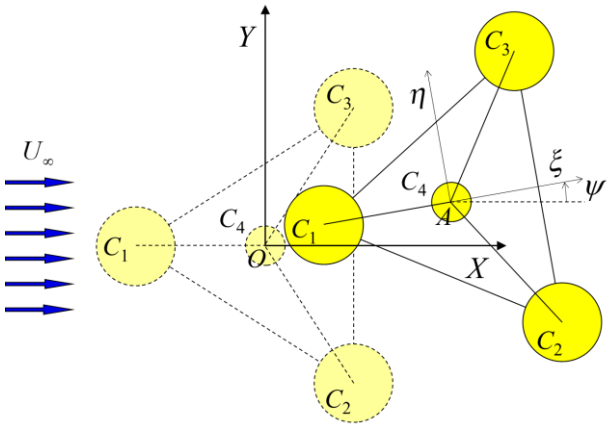

Figure 1. Coordinates and general definitions. At origin, platform is shown at 0 degrees current heading.

The Lagrange's equations of motion for the platform can be expressed as follows:

$$\frac{d}{dt}\left(\frac{\partial T}{\partial \dot{\mathbf{q}}}\right) - \frac{\partial T}{\partial \mathbf{q}} = \mathbf{Q}^m + \mathbf{Q}^v, \tag{1}$$

where T represents the kinetic energy of the system, including added-mass inertial effects; $\mathbf{Q}^m = \left[Q_j^m\right]$ and $\mathbf{Q}^v = \left[Q_j^v\right]$; $j = 1,2,3,$ are, respectively, the generalized forces corresponding to the restoring mooring forces and to the hydrodynamic forces associated to vortex shedding phenomenon effects.

Let $\mathbf{M} = \mathbf{M}_p + \mathbf{M}_a$ be the (3×3) mass matrix, where the subscript p refers to the platform and the subscript a to the classic added mass tensor concept. Also, let $\mathbf{M}_a = \mathbf{B}\hat{\mathbf{M}}_a\mathbf{B}^T$, with $\mathbf{B}$ the rotation matrix from (O,X,Y) to (A,ξ,η), and $\hat{\mathbf{M}}_a$ the added mass tensor expressed in the body-fixed coordinate system (A,ξ,η), which, due to symmetry can be assumed as a diagonal 3×3 matrix. Oscillations at very slow motions are assumed, such that the asymptotic limit for the added mass tensor at zero frequency can be used. Thus, the kinetic energy may be put in the following form:

$$T = \frac{1}{2}\dot{\mathbf{q}}^T\mathbf{M}\dot{\mathbf{q}}. \tag{2}$$

Under the above set of simplifying hypotheses and assuming that the centroid is taken as the center of mass, i.e., $A \equiv G$, the equations of motions (1) will then appear in a rather simple matrix form,

$$\mathbf{M}\ddot{\mathbf{q}} + \mathbf{Q}^I = \mathbf{Q}^m + \mathbf{Q}^v, \tag{3}$$

with $\mathbf{Q}^I$ denoting generalized inertia forces related to the angular velocity of the body.

Phenomenological model and hydrodynamic forces

Considering the diagram shown in Figure 2, adapted from [12], the hydrodynamic forces related to vortex shedding effects can be described in terms of their components in the body-fixed coordinate system. Let U_∞ be the free stream velocity, which is supposed aligned with the axis OX. Let U_k be the instantaneous relative velocity of the current stream with respect to the centroid of the k-th column, being $U_{\xi,k}$ and $U_{\eta,k}$ their projections on the axes ξ and η. Define $F_{L,k}$ and $F_{D,k}$ as 'lift' and 'drag' forces, respectively, the former perpendicular to U_k and the latter aligned with U_k. $F_{v_{\xi,k}}$ and $F_{v_{\eta,k}}$ are the components of the hydrodynamic forces in the directions ξ and η, respectively, and β_k is the angle between the directions of U_k and U_∞.

Considering a platform with N_c columns, such that $k = 1,2,\ldots,N_c$, we then follow [12] and [22], to obtain:

$$\begin{aligned}
F_{v_{\xi,k}} &= \frac{1}{2}\rho D_k H_k C_{\xi,k} U_\infty^2;\ F_{v_{\eta,k}} = \frac{1}{2}\rho D_k H_k C_{\eta,k} U_\infty^2,\\
C_{\xi,k} &= (C_{D,k}U_{\xi,k} - C_{L,k}U_{\eta,k})\frac{U_k}{U_\infty^2},\\
C_{\eta,k} &= (C_{D,k}U_{\eta,k} + C_{L,k}U_{\xi,k})\frac{U_k}{U_\infty^2},\\
U_{\xi,k} &= U_{\infty,\xi} - v_{C_{k,\xi}};\ U_{\eta,k} = U_{\infty,\eta} - v_{C_{k,\eta}};\ U_k = \sqrt{U_{\xi,k}^2 + U_{\eta,k}^2},
\end{aligned} \tag{4}$$

where ρ is the water density, D_k is the diameter of the k-th column and H_k its respective draught; $C_{D,k}$ and $C_{L,k}$ are the hydrodynamic coefficients in their respective directions. The velocity terms are expressed in the local frame, (A,ξ,η), such that $U_{\infty,\xi}$ and $U_{\infty,\eta}$ are the components of the stream velocity, whereas $v_{C_{k,\xi}}$ and $v_{C_{k,\eta}}$ are the components of the velocity vector of the k-th column center, C_k, i.e.:

$$\mathbf{v}_{C_k} = \mathbf{v}_A + \boldsymbol{\omega}_p \times \mathbf{r}_{C_k|A}. \tag{5}$$

In Eq. (5), $\mathbf{v}_A$ is the velocity vector of the centroid of the platform, A, on the horizontal plane, $\boldsymbol{\omega}_p$ is the angular velocity vector of the platform, and $\mathbf{r}_{C_k|A}$ is the relative position vector between A and the center of the k-th column, C_k.

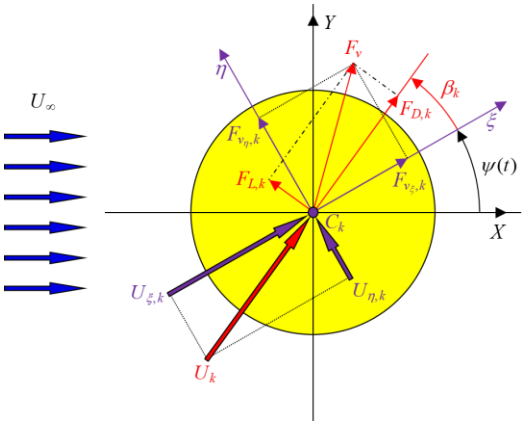

Figure 2. Forces diagram for the k-th column; based on [13], after [12]. Cylinder moving left and down.

On the other hand, $F_{v_{\xi,k}}$ and $F_{v_{\eta,k}}$ may be written,

$$\begin{aligned}
F_{v_{\xi,k}} &= F_{D_k}\cos(\beta_k) - F_{L_k}\sin(\beta_k),\\
F_{v_{\eta,k}} &= F_{D_k}\sin(\beta_k) + F_{L_k}\cos(\beta_k),\\
\cos(\beta_k) &= U_{\xi,k}/U_k;\ \sin(\beta_k) = U_{\eta,k}/U_k.
\end{aligned} \tag{6}$$

Therefore,

$$\begin{aligned}
F_{v_{\xi,k}} &= \frac{1}{2}\rho D_k H_k (C_{D,k}U_{\xi,k} - C_{L,k}U_{\eta,k})U_k,\\
F_{v_{\eta,k}} &= \frac{1}{2}\rho D_k H_k (C_{D,k}U_{\eta,k} + C_{L,k}U_{\xi,k})U_k,
\end{aligned} \tag{7}$$

and the corresponding generalized viscous hydrodynamic force vector turns out to be:

$$Q_j^v = \sum_{k=1}^{N_c}\mathbf{F}_{v,k}\cdot\frac{\partial\mathbf{v}_{C_k}}{\partial\dot{q}_j};\ j = 1,2,3. \tag{8}$$

The wake oscillator model

Following [18], by considering [13]-[14], we write two forced van der Pol oscillators for each column, aligned with the directions ξ and η, being $(a_{\xi,k}, a_{\eta,k})$ the components of the acceleration at the center of the k-th column, in the form:

$$\ddot{w}_{\xi,k} + \varepsilon_\xi \omega_{s,k}(w_{\xi,k}^2 - 1)\dot{w}_{\xi,k} + 4\omega_{s,k}^2 w_{\xi,k} = \frac{A_\xi}{D_k} a_{\xi,k},$$
$$\ddot{w}_{\eta,k} + \varepsilon_\eta \omega_{s,k}(w_{\eta,k}^2 - 1)\dot{w}_{\eta,k} + \omega_{s,k}^2 w_{\eta,k} = \frac{A_\eta}{D_k} a_{\eta,k}, \quad (9)$$

where $\mathbf{w} = \begin{bmatrix} w_{\xi,1} & w_{\eta,1} & \dots & w_{\xi,N_c} & w_{\eta,N_c} \end{bmatrix}^T$ is a hidden generalized coordinator vector that phenomenologically emulates the wake dynamics and its interaction with the structure; ε_ξ and ε_η are damping parameters and $\omega_{s,k} = 2\pi S_{t,k}(U_k / D_k)$ is the shedding frequency, being $S_{t,k}$ a characteristic value of the Strouhal number, specific for the case of low aspect ratio cylinders. Notice that the in-line wake oscillator vibrates with twice the frequency corresponding to the crosswise one. This is a common *ad-hoc* assumption that comes from well-known experimental VIV observations, according to which the fundamental harmonic of drag forces pulsates twice as fast as that of the lift forces. The terms on the r.h.s of Eq. (9) represent the coupling between the wake oscillators and the body equations of motion. According to [8], coupling through inertial terms are recommended, despite original models apply velocity terms; see, e.g., [6]. The inertial coupling has been followed since, by a number of authors, as [12] or [13]. The coefficients $(\varepsilon_\xi, \varepsilon_\eta)$ and (A_ξ, A_η) have been calibrated from experiments, [15], [16], and from CFD simulations, [14].

Finally, the generalized wake forces in Eq. (3) are computed by writing the lift and drag coefficients as functions of the wake variables, [14]-[15], in the form,

$$C_{L,k} = \frac{C_{L0}}{2} w_{\eta,k}; \; C_{D,k} = C_{D0}(1 + K w_{\eta,k}^2) + \frac{C_{D0}^f}{2} w_{\xi,k}, \quad (10)$$

where C_{L0} and C_{D0} are, respectively, the lift and drag coefficients for a fixed cylinder; C_{D0}^f is a weighting coefficient for the oscillation amplitude of the drag; and K is a constant, experimentally determined, [15].

Coupled model

Gathering Eqs. (3-10), the 11-dof reduced-order model may be written in the following form:

$$\tilde{\mathbf{M}}\ddot{\tilde{\mathbf{q}}} = \tilde{\mathbf{Q}}_c + \tilde{\mathbf{Q}}_{nc}, \quad (11)$$

where, on the l.h.s., $\tilde{\mathbf{M}} \in \Re^{11x11}$ and $\tilde{\mathbf{q}} \in \Re^{11}$ are, respectively, the augmented inertia matrix and generalized coordinate vector; and on the r.h.s., $\tilde{\mathbf{Q}}_c \in \Re^{11}$ and $\tilde{\mathbf{Q}}_{nc} \in \Re^{11}$ are, respectively, generalized force vectors, the first one dependent on the generalized configuration of the system and the second one is a non-conservative term. Eq. (12) provides their respective forms explicitly.

$$\tilde{\mathbf{M}} = \begin{bmatrix} \mathbf{M} & \mathbf{0} \\ \mathbf{A}_w & \mathbf{1} \end{bmatrix}; \; \tilde{\mathbf{q}} = \begin{bmatrix} \mathbf{q} \\ \mathbf{w} \end{bmatrix},$$
$$\tilde{\mathbf{Q}}_c = \begin{bmatrix} \mathbf{Q}^m - \mathbf{Q}^I \\ \mathbf{Q}_w^r \end{bmatrix}; \; \tilde{\mathbf{Q}}_{nc} = \begin{bmatrix} \mathbf{Q}^v \\ \mathbf{Q}_w^v \end{bmatrix}, \quad (12)$$

where,

$$\mathbf{A}_w = \begin{bmatrix} -\frac{A_\xi}{D_1}\frac{\partial a_{\xi,1}}{\partial \ddot{q}_1} & -\frac{A_\xi}{D_1}\frac{\partial a_{\xi,1}}{\partial \ddot{q}_2} & -\frac{A_\xi}{D_1}\frac{\partial a_{\xi,1}}{\partial \ddot{q}_3} \\ -\frac{A_\eta}{D_1}\frac{\partial a_{\eta,1}}{\partial \ddot{q}_1} & -\frac{A_\eta}{D_1}\frac{\partial a_{\eta,1}}{\partial \ddot{q}_2} & -\frac{A_\eta}{D_1}\frac{\partial a_{\eta,1}}{\partial \ddot{q}_3} \\ \vdots & \vdots & \vdots \\ -\frac{A_\xi}{D_{N_c}}\frac{\partial a_{\xi,N_c}}{\partial \ddot{q}_1} & -\frac{A_\xi}{D_{N_c}}\frac{\partial a_{\xi,N_c}}{\partial \ddot{q}_2} & -\frac{A_\xi}{D_{N_c}}\frac{\partial a_{\xi,N_c}}{\partial \ddot{q}_3} \\ -\frac{A_\eta}{D_{N_c}}\frac{\partial a_{\eta,N_c}}{\partial \ddot{q}_1} & -\frac{A_\eta}{D_{N_c}}\frac{\partial a_{\eta,N_c}}{\partial \ddot{q}_2} & -\frac{A_\eta}{D_{N_c}}\frac{\partial a_{\eta,N_c}}{\partial \ddot{q}_3} \end{bmatrix}, \quad (13)$$

$$\mathbf{Q}_w^r = \begin{bmatrix} -4\omega_{s,1}^2 w_{\xi,1} \\ -\omega_{s,1}^2 w_{\eta,1} \\ \vdots \\ -4\omega_{s,N_c}^2 w_{\xi,N_c} \\ -\omega_{s,N_c}^2 w_{\eta,N_c} \end{bmatrix}; \; \mathbf{Q}_w^v = \begin{bmatrix} -\varepsilon_\xi \omega_{s,1}(w_{\xi,1}^2 - 1)\dot{w}_{\xi,1} \\ -\varepsilon_\eta \omega_{s,1}(w_{\eta,1}^2 - 1)\dot{w}_{\eta,1} \\ \vdots \\ -\varepsilon_\xi \omega_{s,N_c}(w_{\xi,N_c}^2 - 1)\dot{w}_{\xi,N_c} \\ -\varepsilon_\eta \omega_{s,N_c}(w_{\eta,N_c}^2 - 1)\dot{w}_{\eta,N_c} \end{bmatrix}. \quad (14)$$

A CASE STUDY

To verify the applicability of the model, a case study was carried out considering the reduced scale model (1:72.72) of the OC4 platform with a simplified mooring system composed of 4 springs lines connected to the towing carriage (Figure 3(a)), used by Gonçalves and collaborators, [21]. The model is equipped with three main columns, in an equilateral arrangement, and a fourth and much smaller one, at the center. The results presented herein replicate the experiments in small-scale, where three current incidence angles were considered (0, 90 and 180 degrees), as illustrated in Figure 3(b)-(d). Simulations were carried out at least for 30 reduced velocities, spanning the range $3 < V_R < 24$, what corresponds to the Reynolds number range $8{,}000 < Re < 70{,}000$, for each incidence angle. The simulations were carried out in a MATLAB® environment, numerically integrating the coupled equations in the state space form. A fixed time step of 0.1 seconds was used, applying the 4th order Runge-Kutta algorithm.

The platform main characteristics are shown in Table 1, while the mooring system parameters and those corresponding to the wake oscillators are given in Tables 2 and 3, respectively. Table 4 shows the inertia and stiffness matrices calculated at the trivial equilibrium position for the current incidences considered in the small-scale experiment, while Table 5 shows the three natural periods evaluated at the same trivial equilibrium condition, comparing those experimentally measured with those calculated with the ROM. Notice that at the trivial equilibrium, the oscillation modes are pure ones, uncoupling the (X, Y, ψ) degrees of freedom. As the platform model drifts off from that trivial equilibrium position, mooring stiffnesses change and motions become coupled to each other, hence producing yaw, even if the current is originally aligned with an axis of symmetry.

Table 1. OC4 scaled model parameters; [21].

Parameters	Values
Draught, H (m)	0.275
Arc radius, R (m)	0.490
Columns centers' radius, r (m)	0.397
Diameters, $\{D_1, D_2, D_3, D_4\}$ (m)	{0.165, 0.165, 0.165, 0.090}
Platform's mass matrix, $\mathbf{M}_p$ (kg, kg, kgm²)	diag{36.70, 36.70, 4.00}
Added mass tensor, $\hat{\mathbf{M}}_a$ (kg, kg, kgm²)	diag{21.72, 22.13, 4.39}
Density of water, ρ (kg/m³)	1000

Table 2. Mooring system parameters; [21], [23].

Parameters	Values
Towing car dimensions, $\{W_m, L_m, \Phi_m\}$ (m)	{1.59, 2.40, 0.98}
Natural lengths $\{l_{n_1}, l_{n_2}, l_{n_3}, l_{n_4}\}$ (m)	{0.80, 0.425, 0.80, 0.425}
Spring constants $\{k_1, k_2, k_3, k_4\}$ (N/m)	{7.46, 9.42, 7.46, 9.42}

Table 3. Wake-oscillators parameters; [15], [19].

Parameters	Values
$\{A_\xi, A_\eta\}$	{12, 6}
$\{\varepsilon_\xi, \varepsilon_\eta\}$	{0.30, 0.15}
$\{C_{D0}, C_{L0}, C_{D0}^f, K\}$	{0.70, 0.30, 0.10, 0.05}
Strouhal numbers for each column, $\{S_{t_1}, S_{t_2}, S_{t_3}, S_{t_4}\}$	{0.145, 0.145, 0.145, 0.150}

Table 4. Mass and stiffness matrices at the trivial equilibrium position; [21], [23].

Incidence	0°, 180°	90°
Mass matrix, $\mathbf{M}$ (kg, kg, kgm²)	diag{58.42, 58.83, 8.39}	diag{58.83, 58.42, 8.39}
Mooring stiffness matrix, $\mathbf{K}$ (N/m, N/m, Nm)	diag{26.48, 27.46, 19.22}	diag{26.48, 27.46, 19.22}

Table 5. Natural periods at the trivial equilibrium position; [21], [23].

	Experiment		ROM	
Incidence	0°, 180°	90°	0°, 180°	90°
DOF	T_n (s)	T_n (s)	T_n (s)	T_n (s)
X	9.40	9.40	9.33	9.36
Y	9.60	9.70	9.20	9.16
ψ	4.20	4.20	4.15	4.15

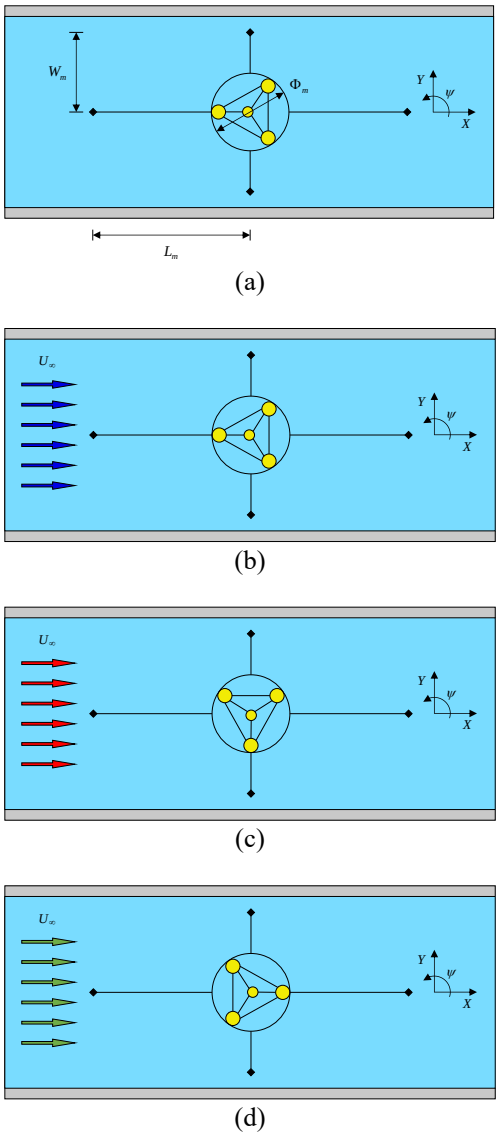

(a)

(b)

(c)

(d)

Figure 3. Experiment sketch with the simplified mooring system. (a): tank sketch and mooring system geometry. (b)-(d): Incoming flow incidence at 0, 90 and 180 degrees.

According to [21], an interesting way to observe the behavior of the platform centroid in the transverse (crosswise) and in-line directions, with respect to the main flow, is by showing its full dynamic response on the horizontal plane. For that, Figures 4 to 6 illustrate the motion of the centroid of the platform on the horizontal plane, obtained with the ROM, for all current incidences considered and for a sample of the reduced velocities of the experiment. The reduced velocity sample was chosen considering the synchronization range of the platform oscillations in the transverse direction and to the yaw angle, which is represented along the trajectory through the color gradient. All simulations started from rest, at the trivial equilibrium position.

Figures 7 to 9 show the comparison between the nondimensional amplitudes obtained with the proposed models of VIM

and the experimental results presented in [21]. Figure 7(a) shows that the proposed model produces a fairly realistic representation of the transverse oscillation amplitude (A_Y / D) for the incidence of 0 degrees, with maximum oscillation amplitude (0.58 at V_R ~ 9), close to the one observed experimentally (0.62 at V_R ~ 8).

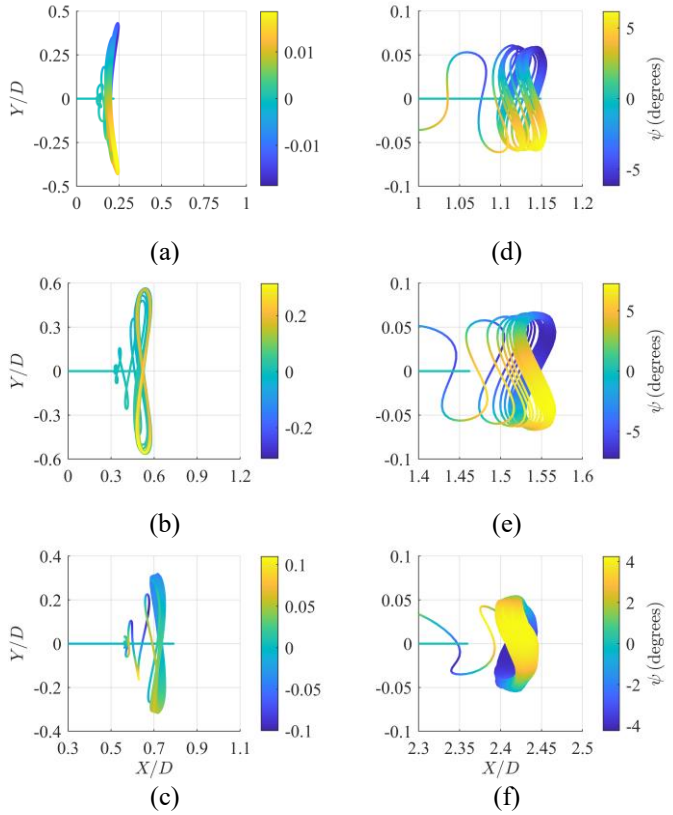

Figure 4. Trajectories of the FOWT's center on the horizontal plane for an incidence angle of 0 degrees (X is the current direction, *in-line*; Y is the direction transversal to it, *cross*). Yaw scaled as in the colored bar. (a): V_R = 5.24; (b): V_R = 8.73; (c): V_R = 11.64; (d): V_R = 14.55; (e): V_R = 16.87; (f): V_R = 22.69.

The synchronization range obtained with the ROM ($5 < V_R < 14$) also approximates well the range observed in the experiments ($4.5 < V_R < 14$).

For the 90 degrees incidence case, the transverse oscillation is fairly well represented, as can be seen in Figure 8(a). In this case, the maximum oscillation amplitude determined with the ROM (0.58 at V_R ~ 8.5) is slightly different from that observed in the experiment (0.51 at V_R ~ 7.9) and the synchronization range predicted by the model ($5 < V_R < 14$) is wider than the one observed experimentally ($5 < V_R < 11$). Possibly, such a behavior is due to the alignment of two columns with the current direction, what certainly increases the hydrodynamic interference between them, not considered in the ROM.

Regarding the amplitude of the in-line oscillation (A_X / D), the model approximates the magnitude of the experimental results, at the beginning of the crosswise oscillation synchronization range, for all the incidence angles analyzed. It should be noticed that at small reduced velocities the wake interference may be conceived as relatively weak. Notice also that the graphs of dominant frequencies reveal, quite clearly, switches between oscillation modes, with jumps occurring at reduced velocities close to 14.

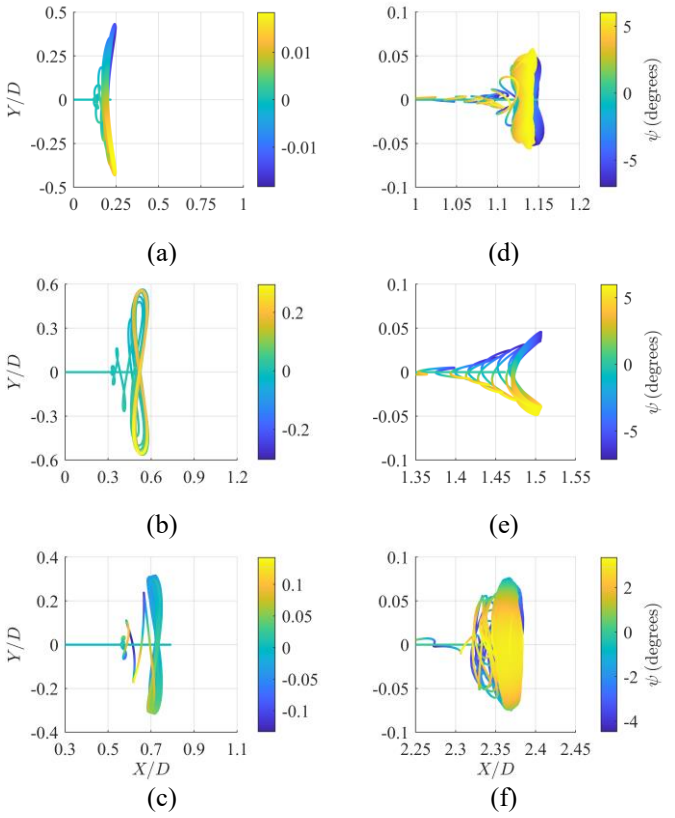

Figure 5. Trajectories of the FOWT's center on the horizontal plane for an incidence angle of 90 degrees (X is the current direction, *in-line*; Y is the direction transversal to it, *cross*). Yaw scaled as in the colored bar. (a): V_R = 5.24; (b): V_R = 8.73; (c): V_R = 11.64; (d): V_R = 14.55; (e): V_R = 16.87; (f): V_R = 22.69.

Concerning the yaw oscillation amplitude (A_ψ) at 0 degrees incidence, Figure 7(c), it is observed that the ROM predicts a maximum value of 7.2 degrees at V_R ~ 18, overestimating by a large amount the typical values found in the experiment, around 2 to 3 degrees. The overprediction is even bigger at 90 and 180 degrees, as depicted in Figures 8(c) and 9(c).

In fact, beyond the main synchronization – the lock-in range for crosswise oscillations – a quite interesting behavior is revealed by the simulations: a resonant response of the yaw angle. Indeed, looking at Table 5, the yawing natural period at the trivial equilibrium position is grossly half the other two. If the graphs of yaw amplitude response and respective dominant frequencies were replotted, by redefining the reduced velocity parameter based on the yaw natural frequency, a VIV-like resonance regime would clearly appear.

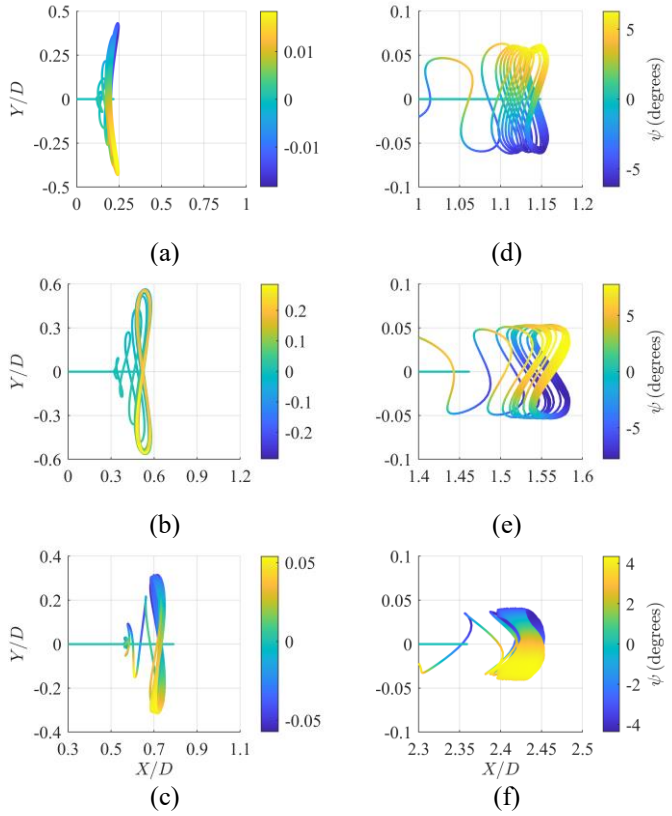

Figure 6. Trajectories of the FOWT's center on the horizontal plane for an incidence angle of 180 degrees (X is the current direction, *in-line*; Y is the direction transversal to it, *cross*). Yaw scaled as in the colored bar. (a): $V_R = 5.24$; (b): $V_R = 8.73$; (c): $V_R = 11.64$; (d): $V_R = 14.55$; (e): $V_R = 16.87$; (f): $V_R = 22.69$.

Notice however that, although an increase trend in the yaw motion may indeed be observed from the small-scale experimental data, there is no clear experimental evidence of a yawing resonant regime. Possibly, the hydrodynamic interference phenomenon, stronger at higher velocities, may have harmed the representation of the ROM, causing the differences observed between the simulation results and the experimental ones. Other possible causes, as the damping effect of the heave plates, could be raised, though.

CONCLUSION

A reduced-order mathematical model was proposed to address the Vortex-Induced Motion, VIM, of a moored (circular) multicolumn floating offshore wind turbine platform. The model is derived considering slow motions on the horizontal plane, at very-low frequencies, such that the asymptotic limit for the added mass tensor at zero frequency can be used. Viscous fluid forces induced by vortex-shedding are modeled through a phenomenological approach, such that the dynamics of the vortex wake that is shed from each cylindrical column is represented through a pair of wake-oscillators, of the van der Pol type.

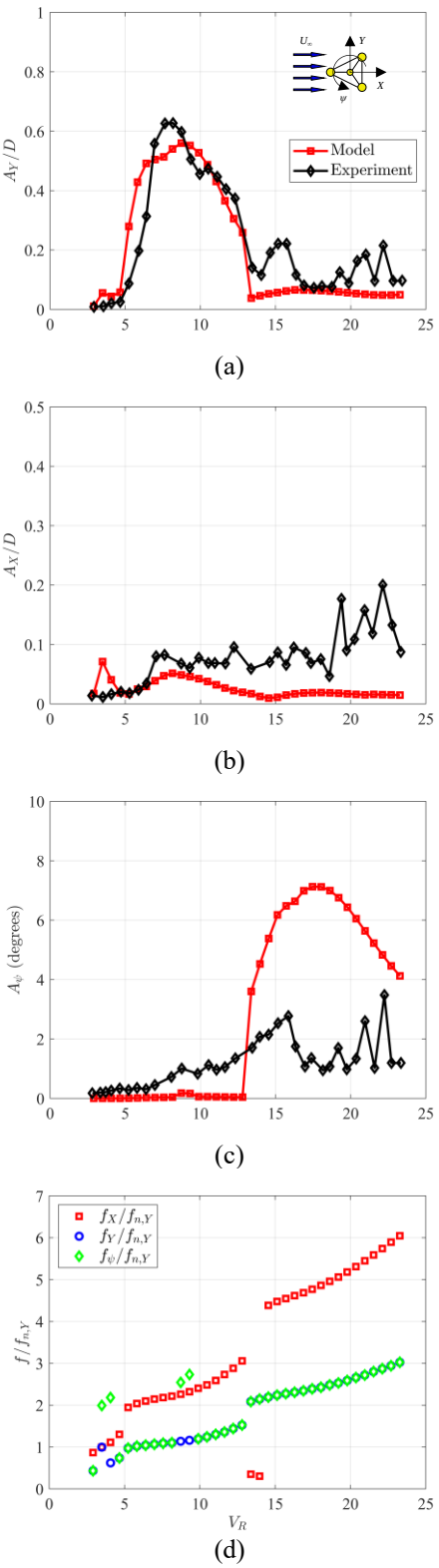

Figure 7. Comparison with experimental results, [21]. Flow at 0 degrees. (a): Cross flow amplitude; (b): In-line amplitude; (c): Yaw amplitude; (d): Dominant nondimensional frequencies.

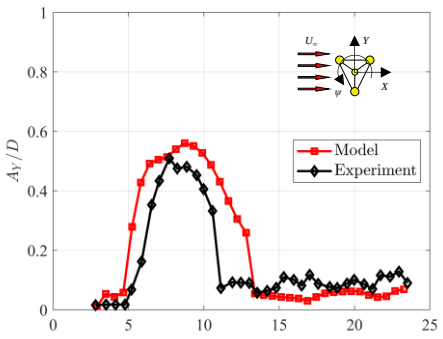

(a)

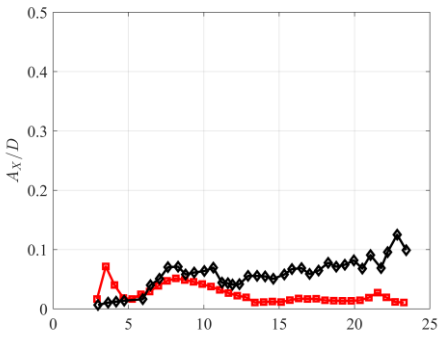

(b)

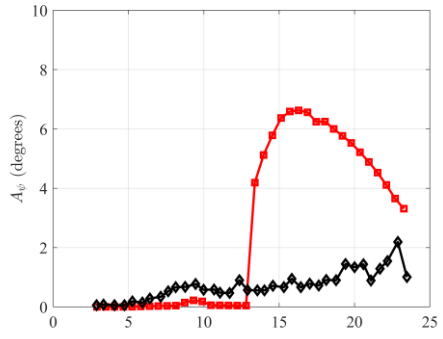

(c)

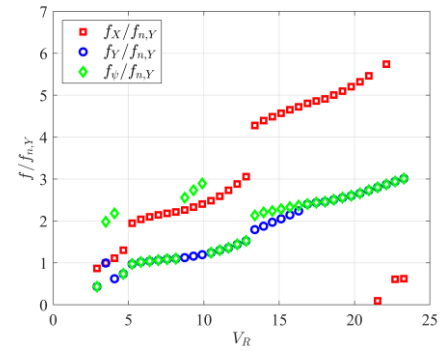

(d)

Figure 8. Comparison with experimental results, [21]. Flow at 90 degrees. (a): Cross flow amplitude; (b): In-line amplitude; (c): Yaw amplitude; (d): Dominant nondimensional frequencies.

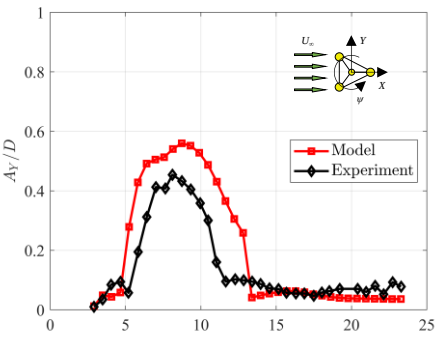

(a)

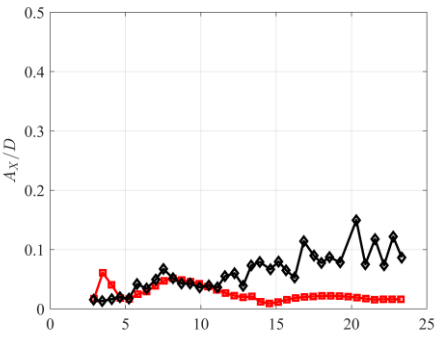

(b)

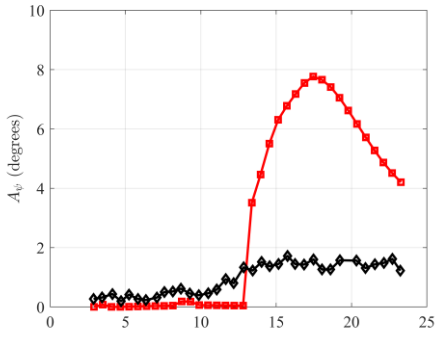

(c)

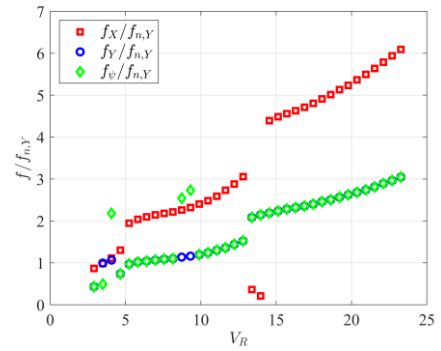

(d)

Figure 9. Comparison with experimental results, [21]. Flow at 180 degrees. (a): Cross flow amplitude; (b): In-line amplitude; (c): Yaw amplitude; (d): Dominant nondimensional frequencies.

Each one of these pairs is considered acting according to the local relative velocity of the incoming flow with respect to the column centroid, in orthogonal directions, aligned with and transversal to it, in the manner proposed by [13], after [12]. All wake interferences that may occur among columns have been simply ignored in the presented version of this ROM, for simplicity. Neither have been considered other possibly relevant hydrodynamic effects as those due to the presence of heave-plates on the flow around the columns, or even due to possibly existent bracings.

Parameters for the wake-oscillators were taken from the technical literature, [14], [15], [16]; particularly, the Strouhal numbers for each column were taken from experimental results with low-aspect ratio cylinders; [19]. Notice that, at a given instant, the differences between local incoming current flow at each column is responsible for producing yawing moments, which would not appear in the case of a monocolumn.

The mooring system action is represented by a conservative non-linear closed-form analytical model, that may take into account any mooring configuration; [20].

It should be noticed that galloping, another phenomenon that might occur in squared section columns platforms might be addressed as well, however not under the wake-oscillator modeling approach.

The development of the present ROM had original motivation from a previous successful model alike, constructed for monocolumn platforms; [18]. In that case, the mooring system had been shown to be responsible for yawing coupling, even treating a circular monocolumn platform. The ROM development was then re-motivated by the experimental findings of current-induced motions for a small-scale model of a FOWT (the OC4 PHASE II FLOATER), reported in [21], at IOWTC2019.

Naturally, a first assessment of the present ROM validity should be carried out by modeling those small-scale experiments, [21]. This has been done. A generally good agreement could be found between crosswise oscillations, at three distinct current incidence angles, 0, 90 and 180 degrees, including amplitudes, synchronization ranges and switching of oscillation modes. A fair agreement was found, considering in-line oscillations inside the crosswise synchronization range. The ROM also revealed something unexpected: the possibility of a resonant behavior of the yaw motion at higher reduced velocities, just after the end of the crosswise synchronization range. Such resonant behavior had not been observed experimentally, however, although trends for moderate yawing amplitudes were reported. Such a point must be deeply investigated.

Finally, it should be stated that, in spite of some differences found in the comparison with the experimental results and despite the quite strong simplifying assumptions adopted in the mathematical modeling of such a complex phenomenon, the preliminary results obtained with the proposed ROM turn it into a very promising approach. Future improvements should involve the effects of wake interferences between columns, dependent on the spacing between them and thought to be an important issue in some incidence angles and at higher reduced velocities. The hydrodynamic effect of the heave plates and braces are other points that certainly deserve further investigation. Parametric sensitivity studies with the ROM are also planned, as those related to initial conditions and initial wake-oscillators phases.

ACKNOWLEDGEMENTS

Authors are truly thankful to Dr. Rodolfo T. Gonçalves, Ocean Space Planning Laboratory, University of Tokyo, for providing data and enlightening discussions. First author acknowledges a PhD scholarship from CAPES. The Petrobras DWFOWT – Deep Water Floating Offshore Wind Turbine project is also acknowledged, for partially supporting the present work and by providing a MSc scholarship to the third author. The second author acknowledges a research grant from CNPq, process 308230/2018-3.

REFERENCES

[1] WindEurope. (2020). *Offshore Wind in Europe. Key trends and statistics 2019.* Brussels, Belgium: WindEurope.

[2] Fujarra, A.L.C, Rosettti, G.F., Wilde, J., Gonçalves, R.T. State-of-Art on Vortex-Induced Motion: A Comprehensive Survey After More than One Decade of Experimental Investigation. ASME 31st Int Conf on Offshore Mechanics and Arctic Engineering, OMAE2012, Rio de Janeiro, 2012.

[3] Aranha, J.A.P. Weak three dimensionality of a flow around a slender cylinder: the Ginzburg-Landau equation. *Journal of the Brazilian Society of Mechanical Sciences and Engineering*, 26, (4): 355-367, 2004.

[4] Huerre, P., Monkewitz, P.A. Local and global instabilities in spatially developing flows. *Annual Rev of Fluid Mechanics*, 22: 473-537, 1990.

[5] Hartlen, R.T., Currie, I.G. Lift oscillator model of vortex induced vibration. *Journal of the Engineering* Mechanics, 96 (5): 577-591, 1970.

[6] Iwan, W. D. and Blevins, R. D. A model for vortex induced oscillation of structures. *J Appl Mech*, 41: 581-586, 1974.

[7] Skop, R.A., Balasubramanian, S. A new twist on an old model for Vortex-Induced Vibration. *Journal of Fluids and Structures*, 11 (4): 395-412, 1997.

[8] Facchinetti, M.L., de Langre, Biolley, F. Coupling of structure and wake oscillators in vortex-induced vibrations. *Journal of Fluids and Structures*, 19 (2): 123-140, 2004.

[9] Fujarra, A., Pesce, C.P. Added mass variation and van der pol models applied to vortex-induced vibrations. *ASME 2*002 Int Mechanical Engineering Congress and Exposition, 207-211, New Orleans, 2002.

[10] Cunha, L.D., Pesce, C.P., Wanderley, J., Fujarra, A.L.C. The robustness of added mass in VIV models. ASME 25th Int Conf on Offshore Mechanics and Arctic Engineering, OMAE2006-92323, Hamburg, June 4-9, 2006.

[11] Bernitsas, M.M., Ofuegbe, J., Chen, Jau-Uei, Sun, H. Eigen-Solution for Flow Induced Oscillations (VIV and Galloping) Revealed at the Fluid-Structure Interface. ASME 2019 38th

Int Conf on Ocean, Offshore and Arctic Engineering. Glasgow, Scotland, UK. June 9–14, 2019.
[12] Ogink, R.H.M., Metrikine, A.V. A wake oscillator with frequency dependent coupling for the modeling of vortex-induced vibration. J Sound and Vibration, 329 (26): 5452-5473, 2010.
[13] Franzini, G.R., Bunzel, L.O. A numerical investigation on piezoelectric energy harvesting from Vortex-Induced Vibrations with one and two degrees of freedom. J Fluids and Structures, 77: 196-212, 2018.
[14] Postnikov, A., Pavlovskaia, E., Wiercigroch, M. 2-dof CFD calibrated wake oscillator model to investigate vortex-induced vibrations. Int J of Mech Sciences 127: 176-190, 2017.
[15] Rosetti, G.F., Fujarra, A.L.C., Nishimoto, K., Ferreira, M.D. A phenomenological model for vortex-induced motions of the monocolumn platform and comparison with experiments. ASME 2009 28th Int Conf on Ocean, Offshore and Arctic Engineering, 2009.
[16] Rosetti, G.F., Gonçalves, R.T., Fujarra, A.L.C., Nishimoto, K. Parametric Analysis of a Phenomenological Model for Vortex-Induced Motions of Monocolumn Platforms. J of the Brazilian Soc of Mechanical Sciences and Engineering, 33 (6): 139-146, 2011.
[17] Gonçalves, R.T., Matsumoto, F.T., Malta, E., Rosetti, G.F., Fujarra, A.L.C., Nishimoto, K. Evolution of the MPSO (monocolumn production, storage and offloading system). Marine Systems & Ocean Technology, 6: 45-53, 2010.
[18] Pesce, B.A., Lins de Oliveira, E., Pesce, C.P. Vortex Induced Motions of a Moored Monocolumn Platform. Proceedings of the XVIII International Symposium on Dynamic Problems of Mechanics, Buzios, 2019.
[19] Gonçalves, R.T., Franzini, G.R., Rosetti, G.F., Meneghini, J.R., Fujarra, A.L.C. Flow around circular cylinders with very low aspect ratio. J Fluids and Structures, 54: 122-141, 2015.
[20] Pesce, C.P., Amaral, G.A., Franzini, G.R. Mooring System Stiffness: A general analytical formulation with an application to Floating Offshore Wind Turbines. ASME 2018 1st International Offshore Wind Technical Conference, IOWTC2018, San Francisco, 2018.
[21] Gonçalves, R.T., Chame, M.E., Silva, L.S.P., Koop, A., Hirabayashi, S., Suzuki, H. Experimental study on flow-induced motions (FIM) of a floating offshore wind turbine semi-submersible type (OC4 PHASE II FLOATER). Proceedings of the ASME 2019 2nd International Offshore Wind Technical Conference, IOWTC2019, Malta, 2019.
[22] Slingsby, M.J. Dynamic interaction of subsea pipeline spans due to vortex-induced vibrations. Master's Thesis, TUDelft, 161 p., 2015.
[23] Gonçalves, R.T., Private communication with the authors, 2019.

APPENDIX

We apply the approach introduced in [20]. In that paper, a generic mooring system is considered and a model for the corresponding generalized restoring forces on the horizontal plane is constructed geometrically, under the formalism of Analytical Mechanics. Figure 10 shows a sketch of the mooring configuration used in the experimental campaign [21]. Four linear springs are attached to a rigid circular ring and to the towing car. The actions of the springs are considered on the horizontal plane. P_i and A_i, $i=1,\ldots,N$, are respectively, the projections of fair-leads and anchors on the plane. $r_i = \overline{A_i P_i} = |A_i - P_i|$ are the distances between P_i and A_i; $\beta_i = const$, the angle between $P_i A$ and the body axis, $A\xi$. Finally, $R_i = R = const$, $i=1,\ldots,N$, due to symmetry.

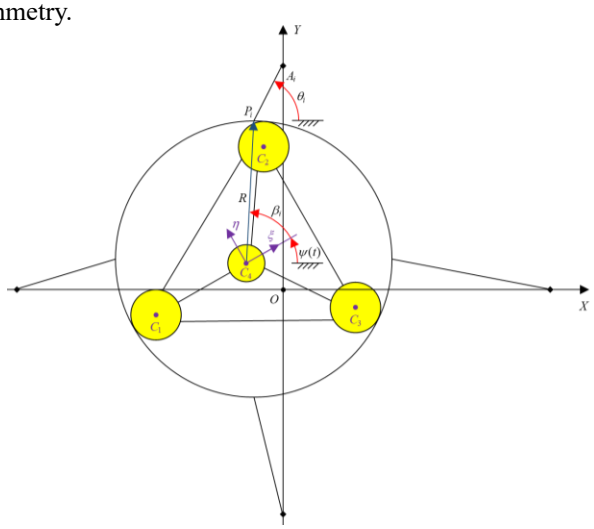

Figure 10. Mooring system sketch and general definitions for the experimental campaign [21]; adapted from [20]; $N=4$.

The generalized restoring mooring forces are written, [20],

$$Q_j^m = \sum_{i=1}^{N} \mathbf{F}_i \cdot \frac{\partial P_i}{\partial q_j}; \quad j=1,2,3; \quad i=1,\ldots,N, \tag{15}$$

where

$$\mathbf{e}_i = \frac{(A_i - P_i)}{r_i} = \begin{bmatrix} \cos\theta_i & \sin\theta_i \end{bmatrix}^T; \quad i=1,\ldots,N, \tag{16}$$

are unit director vectors on the horizontal plane and

$$\mathbf{F}_i = \mathbf{F}_i(r_i) = f_i(r_i)\mathbf{e}_i; \quad i=1,\ldots,N, \tag{17}$$

the horizontal components of tension provided by each one of the linear springs. The restoring force intensities are supposed to be linear functions of position only, in the form $f(r_i)$, no friction or viscous effects considered, in a quasi-static and simplified approach. Moreover, since each fair-lead position on the horizontal plane,

$$(P_i - O) = \begin{bmatrix} x + R_i\cos(\psi+\beta_i) & y + R_i\,\mathrm{sen}(\psi+\beta_i) \end{bmatrix}^T, \tag{18}$$

is a function of the generalized coordinates vector $\mathbf{q}$, the generalized restoring mooring force vector may be also written as a function $\mathbf{Q}^m = \mathbf{Q}^m(\mathbf{q};\Pi)$, where $\Pi = \{(A_i \;\; R_i \;\; \beta_i); i=1,\ldots,N\}$ is the set of geometrical parameters.